ARTICLE TEMPLATE

A non-local damage model for the fatigue behavior of metallic polycrystals

Charles Mareau[a]

[a]LAMPA - Arts et Métiers ParisTech, 2 boulevard du Ronceray, 49035 Angers, France

ARTICLE HISTORY
Compiled October 25, 2019

ABSTRACT

The development of fatigue damage in metallic materials is a complex process influenced by both intrinsic (e.g. texture, defects) and extrinsic (e.g. loading mode, frequency) factors. To better understand this process, some efforts have been made to develop microstructure-sensitive models that consider the impact of microstructural heterogeneities on the formation of fatigue cracks. An important limitation of such models is their inability to describe the transition between the nucleation and growth stages in a consistent thermodynamic framework. To circumvent this limitation, a constitutive model, which is appropriate for the description of both nucleation and early growth, is proposed. For this purpose, non-local damage mechanics is used to construct a set of constitutive relations that explicitly considers the progressive stiffness reduction due to the formation of fatigue cracks. Specifically, a damage variable is attached to each slip system, which allows considering both the anisotropic aspect of fatigue damage and closure effects. The spatial gradients of the damage variables are treated as additional state variables to account for the increase of surface energy associated with the formation of fatigue cracks. For the evolution equations to be compatible with the second law of thermodynamics, a modified form of the entropy production inequality is adopted. For illustration purposes, the non-local damage model is implemented in a spectral solver. Some numerical examples are then presented. These examples allow discussing the ability of the proposed model to describe the impact of loading conditions and pre-existing defects on the fatigue behavior of metallic polycrystals.

KEYWORDS
Damage; fatigue; polycrystalline metals; thermodynamics; FFT

1. Introduction

For metallic materials, microstructural features (e.g. grains, pores) strongly impact the process driving to the initiation and the propagation of short fatigue cracks [1, 2]. Indeed, depending on loading conditions, microstructural heterogeneities possibly act as stress concentrators leading to the initiation of fatigue cracks. To investigate the impact of both loading conditions and microstructural features, significant efforts have been made to develop so-called microstructure-sensitive models [3]. For the specific case of fatigue crack initiation, these models use some indicators, often inspired by fatigue criteria (e.g. Dang Van [4], Fatemi-Socie [5]), to determine whether the conditions for

CONTACT Charles Mareau. Email: charles.mareau@ensam.eu

initiation are met are not [6–9]. The problem of crack growth is more complex, mostly because it requires dealing with the extension of the crack front. A methodology for the growth of short cracks has been proposed by Castelluccio *et al.* [10]. It consists in assuming the growth rate to be related to the crack tip displacement range, which is itself connected to the indicator used for crack initiation. This approach has been used to study the fatigue behavior of a Ni-based superalloy [11].

Continuum damage mechanics [12] provides an alternative framework for the evaluation of the impact of microstructural features on the fatigue behavior of metallic materials [13–15]. The idea consists in introducing some damage variables to explicitly account for the progressive degradation of mechanical resistance caused by the development of fatigue cracks. In comparison with other approaches, damage-based models can be formulated using the concept of internal state variables [16] and hence be constructed in a consistent thermodynamic framework. However, the development of damage is often accompanied by a spatial localization phenomenon, so that numerical solutions to damage problems do not necessarily converge upon mesh refinement [17]. Though this approach has been little employed in the context of fatigue, the difficulties associated with localization can be circumvented with gradient damage models. The spatial gradients of damage variables, which are treated as additional state variables, serve regularization purposes and allow considering the surface energy associated with cracks. The classical treatment of gradient damage models uses an extended version of the principle of virtual power, which consists in treating the damage variable and its gradient as external state variables [18]. An alternative approach, suggested by Maugin [19], relies on the adoption of a modified version of the entropy production inequality, which includes an extra contribution to the entropy flow. With this strategy, both the damage variable and its gradient are treated as internal state variables.

In this work, a non-local damage model is constructed to describe the nucleation and the early growth of fatigue cracks in metallic materials. The development of constitutive relations uses the framework of crystal plasticity and the extra entropy flow concept of [19]. These relations are then implemented within a spectral solver that allows solving equilibrium and compatibility equations.

This paper is organized as follows. In the first section, the field equations governing the thermomechanical behavior of solids are briefly recalled. Particular attention is paid to the definition of the extra entropy flow. The construction of constitutive relations, within the framework of continuum thermodynamics [20], is detailed in the second section. The implementation of constitutive equations in a spectral (i.e. FFT) solver is briefly described in the third section. For illustration purposes, some applications of the proposed model are shown in the final section.

2. Field equations

In this section, the fundamental equations governing the thermomechanical behavior of solids are recalled. For this purpose, a deformable body $\mathcal{B}$ consisting of a collection of crystallites being perfectly bonded across their interfaces is considered. As shown in Figure 1, $\mathscr{V}_0$ is the region occupied by the material points of $\mathcal{B}$ in the reference configuration.

For a material point, whose position in the reference configuration is denoted by $\boldsymbol{X}$, the position $\boldsymbol{x}$ and temperature T at time t are given by:

$$\boldsymbol{x} = \boldsymbol{\chi}\left(\boldsymbol{X}, t\right), \; T = \theta\left(\boldsymbol{X}, t\right) \tag{1}$$

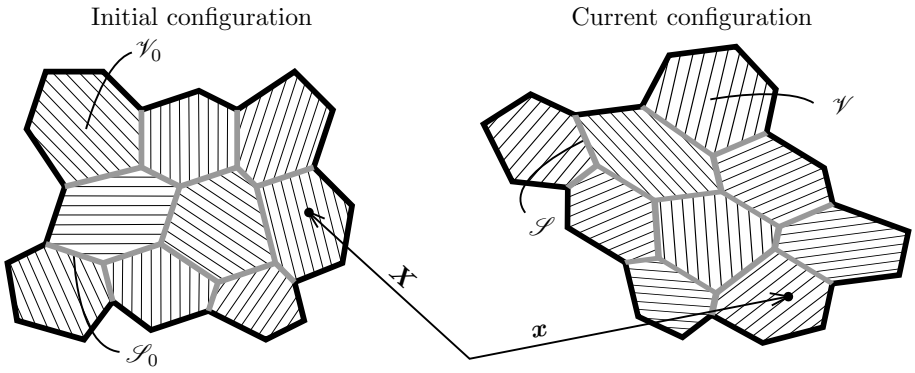

Figure 1. Motion of a body $\mathcal{B}$ consisting of a collection of crystallites.

where $\boldsymbol{\chi}$ and θ are functions defining the motion and temperature histories. Because of the interfaces separating different crystallites, $\boldsymbol{\chi}$ and θ are continuous but only piecewise differentiable functions. In the following, the singular surface formed by grain boundaries in the reference configuration is denoted by $\mathscr{S}_0$.

The deformation gradient tensor $\boldsymbol{F}$ is determined from the function $\boldsymbol{\chi}$ according to[1]:

$$\boldsymbol{F} = \boldsymbol{\chi} \otimes \boldsymbol{\nabla},\ \boldsymbol{X} \in \mathscr{V}_0 \backslash \mathscr{S}_0 \tag{2}$$

$$[\boldsymbol{F}] = \boldsymbol{\beta} \otimes \boldsymbol{N},\ \boldsymbol{X} \in \mathscr{S}_0 \tag{3}$$

In the above equation, which is a necessary condition for kinematical compatibility, the vector-valued function $\boldsymbol{\beta}$ represents the amplitude of the jump for the gradient of $\boldsymbol{\chi}$ across an interface with unit normal $\boldsymbol{N}$.

The evolution of the deformable body $\mathcal{B}$ is bound by the restrictions imposed by basic mechanical and thermodynamical principles. The balance equations resulting from these restrictions are now recalled in a material form. First, the balance equations associated with mass conservation equation are:

$$\dot{\rho}_0 = 0,\ \boldsymbol{X} \in \mathscr{V}_0 \backslash \mathscr{S}_0 \tag{4}$$

$$[\dot{\rho}_0] = 0,\ \boldsymbol{X} \in \mathscr{S}_0 \tag{5}$$

where ρ_0 is the mass density in the reference configuration.

Second, for any material point, the conservation of linear and angular momenta imposes:

$$\boldsymbol{P} \cdot \boldsymbol{\nabla} + \boldsymbol{B} = \rho_0 \ddot{\boldsymbol{x}},\ \boldsymbol{X} \in \mathscr{V}_0 \backslash \mathscr{S}_0 \tag{6}$$

$$\boldsymbol{P} \cdot \boldsymbol{F}^T = \boldsymbol{F} \cdot \boldsymbol{P}^T,\ \boldsymbol{X} \in \mathscr{V}_0 \backslash \mathscr{S}_0 \tag{7}$$

$$[\boldsymbol{P}] \cdot \boldsymbol{N} = \boldsymbol{0},\ \boldsymbol{X} \in \mathscr{S}_0 \tag{8}$$

where $\boldsymbol{B}$ is the body force density and $\boldsymbol{P}$ is the first Piola-Kirchoff stress tensor.

[1] $[\bullet]$ denotes the jump of $\bullet$ across an interface.

According to the first law of thermodynamics, the change in total (internal and kinetic) energy is equal to the sum of the power developed by external forces and the total heat flux. The local form of the balance of energy is therefore written as follows:

$$\rho_0 \dot{u} = \boldsymbol{P} : \dot{\boldsymbol{F}} - \boldsymbol{\nabla} \cdot \boldsymbol{Q} + \rho_0 r, \; \boldsymbol{X} \in \mathscr{V}_0 \backslash \mathscr{S}_0 \tag{9}$$

$$[\boldsymbol{Q}] \cdot \boldsymbol{N} = 0, \; \boldsymbol{X} \in \mathscr{S}_0 \tag{10}$$

where u is the specific internal energy, $\boldsymbol{Q}$ is the heat flux vector and r is the specific heat supply.

The second law of thermodynamics requires the net entropy production to be non-negative. The corresponding local statement is given by the following inequalities:

$$\rho_0 \dot{s} + \boldsymbol{\nabla} \cdot \boldsymbol{J} - \rho_0 z \geq 0, \; \boldsymbol{X} \in \mathscr{V}_0 \backslash \mathscr{S}_0 \tag{11}$$

$$[\boldsymbol{J}] \cdot \boldsymbol{N} = 0, \; \boldsymbol{X} \in \mathscr{S}_0 \tag{12}$$

where s is the specific entropy, $\boldsymbol{J}$ is the entropy flux and z is the specific entropy supply. In the present work, a non-classical definition of the entropy flow is adopted. Indeed, following of the suggestion of Maugin [19], an extra contribution to the entropy flow is considered:

$$\boldsymbol{J} = \frac{\boldsymbol{Q}}{T} \tag{13}$$

$$z = \frac{r}{T} + \frac{h}{T} \tag{14}$$

While the original suggestion of Maugin [19] uses an extra entropy flux, the approach of Ireman and Nguyen [21], which uses an extra supply of entropy h/T, is preferred here. The classical definition of the entropy flux $\boldsymbol{J} = \boldsymbol{Q}/T$ is thus preserved but an appropriate constitutive relation for the extra entropy supply h/T is needed. This aspect is detailed in the following section.

3. Constitutive relations

3.1. Multiplicative decomposition

The balance equations, which have been listed in the above section, are not sufficient for determining the evolution of the deformable body, so that additional constitutive equations are required. For the purpose of presenting these relations, a single material point is considered for now. For such a material point, as suggested by [22], the following multiplicative decomposition of the deformation gradient tensor $\boldsymbol{F}$ is adopted:

$$\boldsymbol{F} = \boldsymbol{F}_\theta \cdot \boldsymbol{F}_p \tag{15}$$

where $\boldsymbol{F}_\theta$ (respectively $\boldsymbol{F}_p$) represents the thermoelastic (respectively plastic) contribution to deformation.

In the present work, plastic deformation solely results from crystallographic slip on a set of n slip systems. As shown in Figure 2, each slip system s is defined in the relaxed isoclinic configuration from two orthogonal unit vectors: the slip plane normal $\boldsymbol{n}_s$ and the slip direction $\boldsymbol{m}_s$. For convenience, a third unit vector $\boldsymbol{k}_s = \boldsymbol{n}_s \times \boldsymbol{m}_s$ is also introduced.

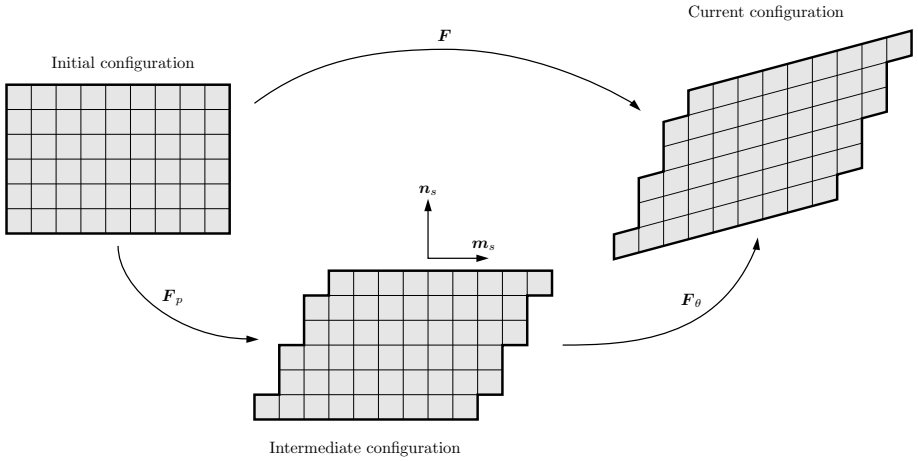

Figure 2. Multiplicative decomposition of the deformation gradient tensor.

Using the above multiplicative decomposition, the Green-Lagrange strain tensor $\boldsymbol{E}$ can be separated into thermoelastic and plastic contributions:

$$\boldsymbol{E} = \frac{1}{2}\left(\boldsymbol{F}^T \cdot \boldsymbol{F} - \boldsymbol{1}\right) \tag{16}$$

$$= \boldsymbol{F}_p^T \cdot \tilde{\boldsymbol{E}}_\theta \cdot \boldsymbol{F}_p + \boldsymbol{E}_p \tag{17}$$

with:

$$\tilde{\boldsymbol{E}}_\theta = \frac{1}{2}\left(\boldsymbol{F}_\theta^T \cdot \boldsymbol{F}_\theta - \boldsymbol{1}\right) \tag{18}$$

$$\boldsymbol{E}_p = \frac{1}{2}\left(\boldsymbol{F}_p^T \cdot \boldsymbol{F}_p - \boldsymbol{1}\right) \tag{19}$$

In a similar fashion, the velocity gradient tensor $\boldsymbol{L}$ can be decomposed as follows:

$$\boldsymbol{L} = \dot{\boldsymbol{F}} \cdot \boldsymbol{F}^{-1} \tag{20}$$

$$= \boldsymbol{L}_\theta + \boldsymbol{F}_\theta \cdot \tilde{\boldsymbol{L}}_p \cdot \boldsymbol{F}_\theta^{-1} \tag{21}$$

with:

$$\boldsymbol{L}_\theta = \dot{\boldsymbol{F}}_\theta \cdot \boldsymbol{F}_\theta^{-1} \tag{22}$$

$$\tilde{\boldsymbol{L}}_p = \dot{\boldsymbol{F}}_p \cdot \boldsymbol{F}_p^{-1} \tag{23}$$

It is emphasized that both $\tilde{\boldsymbol{E}}_\theta$ and $\tilde{\boldsymbol{L}}_p$ are invariant tensors associated with the intermediate configuration. The stress tensors $\tilde{\boldsymbol{S}}$ and $\tilde{\boldsymbol{\Sigma}}$, which are the power conjugates to $d\tilde{\boldsymbol{E}}_\theta/dt$ and $\tilde{\boldsymbol{L}}_p$, can be obtained from the density of power developed by internal forces. Indeed, the density of power developed by internal forces can be decomposed into thermoelastic and plastic contributions as follows:

$$\boldsymbol{P} : \dot{\boldsymbol{F}} = \tilde{\boldsymbol{S}} : \dot{\tilde{\boldsymbol{E}}}_\theta + \tilde{\boldsymbol{\Sigma}} : \tilde{\boldsymbol{L}}_p \tag{24}$$

Table 1. Pairs of conjugate state variables used for the development of the present constitutive model.

State variable	Conjugate variable
T	$-s$
$\tilde{\boldsymbol{S}}$	$-\tilde{\boldsymbol{E}}_\theta$
α_s	X_s
ϱ_s	R_s
ϕ_s	Y_s
$\boldsymbol{\nabla}\phi_s$	$\boldsymbol{G}_s$

In the above expression, $\tilde{\boldsymbol{S}}$ is the second Piola-Kirchoff stress tensor attached to the isoclinic intermediate configuration. It is connected to the first Piola-Kirchoff stress tensor $\boldsymbol{P}$ according to:

$$\tilde{\boldsymbol{S}} = \boldsymbol{F}_\theta^{-1} \cdot \boldsymbol{P} \cdot \boldsymbol{F}_p^{T} \tag{25}$$

The expression of the Mandel stress tensor $\tilde{\boldsymbol{\Sigma}}$, which is the power conjugate to $\tilde{\boldsymbol{L}}_p$, is:

$$\tilde{\boldsymbol{\Sigma}} = \boldsymbol{F}_\theta^{T} \cdot \boldsymbol{P} \cdot \boldsymbol{F}_p^{T} \tag{26}$$

3.2. State equations

At a given time t, the state of the material point is uniquely defined from a set of state variables that are listed in Table 1 with their corresponding dual variables. The external state variables are the stress tensor $\tilde{\boldsymbol{S}}$ and the absolute temperature T. For the description of the cyclic behavior, some additional internal state variables are introduced. First, a kinematic hardening variable α_s and an isotropic hardening variable ϱ_s are associated to each slip system s (with $s = 1$ to n). To describe the degradation of mechanical properties, a damage variable ϕ_s (with $0 \leq \phi_s \leq 1$) is attached to each slip system s. The case where ϕ_s is equal to zero corresponds to the absence of damage on the corresponding slip system. At the opposite, a slip system for which ϕ_s takes a unity value is fully damaged and unable to transmit internal forces. The association of a damage variable to each slip system is particularly well-suited for the modelling of stage I cracks that propagate along slip systems with maximum resolved shear stresses [23]. Also, for regularization purposes, the spatial gradients $\boldsymbol{\nabla}\phi_s$ of the above damage variables are considered as internal variables.

The specific Gibbs free energy g is a state function of the aforementioned state variables that is related to the specific internal energy u according to:

$$g = u - sT - \frac{\tilde{\boldsymbol{S}} : \tilde{\boldsymbol{E}}_\theta}{\rho_0} \tag{27}$$

In the present work, the following decomposition of the specific Gibbs free energy g is adopted:

$$g\left(\tilde{\boldsymbol{S}}, T, \phi_s, \boldsymbol{\nabla}\phi_s, \alpha_s, \varrho_s\right) = g_\theta\left(\tilde{\boldsymbol{S}}, T, \phi_s\right) + g_{th}\left(T\right) + g_k\left(\alpha_s\right) + g_i\left(\varrho_s\right) + g_d\left(\phi_s, \boldsymbol{\nabla}\phi_s\right) \tag{28}$$

In the above decomposition, the impact of damage variables on the thermoelastic contribution g_θ is introduced to model the stiffness reduction associated with the for-

mation of fatigue cracks. The thermal contribution to free energy, which solely depends on the absolute temperature T, is given by g_{th}. Also, the contribution g_k represents the stored energy resulting from the internal stresses responsible for kinematic hardening. In a similar fashion, the stored energy associated with the crystalline defects contributing to isotropic hardening (e.g. dislocations) is included in g_i. Finally, the contribution g_d, which depends on the damage variables and their gradients, aims at considering the increase of surface energy associated with the formation of fatigue cracks.

The thermoelastic contribution g_θ to free energy is given by:

$$g_\theta\left(\tilde{\boldsymbol{S}}, T, \phi_s\right) = -\frac{1}{2\rho_0}\tilde{\boldsymbol{S}} : \mathbb{S}\left(\tilde{\boldsymbol{S}}, \phi_s\right) : \tilde{\boldsymbol{S}} - \frac{1}{\rho_0}\tilde{\boldsymbol{S}} : \boldsymbol{\alpha}\left(T - T_0\right) \tag{29}$$

where $\mathbb{S}$ is the damage-dependent elastic compliance tensor (with $\mathbb{C} = \mathbb{S}^{-1}$), $\boldsymbol{\alpha}$ is the thermal expansion tensor and T_0 is a reference temperature. Following the idea of [15], the dependence of the elastic compliance tensor $\mathbb{S}$ to the damage variables ϕ_s is such that:

$$\mathbb{S}\left(\tilde{\boldsymbol{S}}, \phi_s\right) = \mathbb{S}_0 + \sum_s \omega\left(\phi_s\right)\left(U\left(\sigma_s\right) A_{nn}\mathbb{N}^s_{nn} + A_{nm}\mathbb{N}^s_{nm} + A_{nk}\mathbb{N}^s_{nk}\right) \tag{30}$$

where $\mathbb{S}_0$ is the initial elastic compliance tensor, U is the unit step function, $\sigma_s = \boldsymbol{n}_s \cdot \tilde{\boldsymbol{S}} \cdot \boldsymbol{n}_s$ is the normal stress acting on the sth slip system and ω is a degradation function with the following properties:

$$\omega\left(0\right) = 0 \tag{31}$$

$$\omega\left(1\right) = \infty \tag{32}$$

In this work, the following expression is chosen for the degradation function ω:

$$\omega\left(\phi_s\right) = \frac{\phi_s}{1 - \phi_s} \tag{33}$$

The fourth-rank projection tensors $\mathbb{N}^s_{nn}$, $\mathbb{N}^s_{nm}$ and $\mathbb{N}^s_{nk}$ are introduced in (30) to account for the anisotropic aspect of fatigue damage. These tensors are defined for each slip system s from:

$$\mathbb{N}^s_{nn} = \boldsymbol{n}_s \otimes \boldsymbol{n}_s \otimes \boldsymbol{n}_s \otimes \boldsymbol{n}_s \tag{34}$$

$$\mathbb{N}^s_{nm} = \frac{1}{4}\left(\boldsymbol{n}_s \otimes \boldsymbol{m}_s + \boldsymbol{m}_s \otimes \boldsymbol{n}_s\right) \otimes \left(\boldsymbol{n}_s \otimes \boldsymbol{m}_s + \boldsymbol{m}_s \otimes \boldsymbol{n}_s\right) \tag{35}$$

$$\mathbb{N}^s_{nk} = \frac{1}{4}\left(\boldsymbol{n}_s \otimes \boldsymbol{k}_s + \boldsymbol{k}_s \otimes \boldsymbol{n}_s\right) \otimes \left(\boldsymbol{n}_s \otimes \boldsymbol{k}_s + \boldsymbol{k}_s \otimes \boldsymbol{n}_s\right) \tag{36}$$

As will be discussed below, A_{nn}, A_{nm} and A_{nk} are material parameters controlling the impact of opening and sliding modes (modes I, II or III) on crack propagation. The expression of the elastic compliance tensor has been constructed to describe the progressive decrease of stiffness properties associated with the development of fatigue damage on a given slip system. Indeed, according to expression (30), when a slip system s is fully damaged, the material point is infinitely compliant along $\boldsymbol{n}_s$. The only exception to this situation is when closure effects are activated. In this specific

case, which occurs when the normal stress σ_s acting on the slip system s is negative, stiffness properties are partly recovered.

The thermal contribution g_{th} to free energy is given by:

$$g_{th}(T) = -\frac{1}{2}\boldsymbol{\lambda} : \boldsymbol{\alpha}\frac{(T-T_0)^2}{T_0} + c\left(T - T_0 - T\ln\frac{T}{T_0}\right) \tag{37}$$

where c is the specific heat capacity and $\boldsymbol{\lambda} = \mathbb{C}_0 : \boldsymbol{\alpha}\ T_0/\rho_0$ is the latent heat tensor.

The contribution of kinematic hardening g_k to free energy is assumed to have the following form:

$$g_k(\alpha_s) = \frac{1}{2\rho_0}C\sum_s \alpha_s^2 \tag{38}$$

where C is the kinematic hardening modulus.

A simple approximation for the contribution of isotropic hardening to free energy consists of assuming:

$$g_i(\varrho_s) = \frac{1}{\rho_0}\frac{1}{N+1}H\sum_s \varrho_s^{N+1} \tag{39}$$

where H is the isotropic hardening modulus and N is the strain hardening exponent.

Finally, for the contribution g_d, which is solely attributed to damage, a scalar variable D is introduced to represent the progression of damage. The damage variable D is defined by:

$$D = \frac{\sum_s \omega(\phi_s)}{1 + \sum_s \omega(\phi_s)} \tag{40}$$

According to the above definition, the damage variable D is equal to zero in the absence of damage and tends toward unity when at least one system is fully damaged. Also, the gradient of the damage variable $\boldsymbol{\nabla} D$ with respect to the initial position $\boldsymbol{X}$ is given by:

$$\boldsymbol{\nabla} D = \sum_s D_{,\phi_s}\boldsymbol{\nabla}\phi_s \tag{41}$$

with:

$$D_{,\phi_s} = (1-D)^2\,\omega_{,\phi_s} \tag{42}$$

$$= \frac{(1-D)^2}{(1-\phi_s)^2} \tag{43}$$

For the damage contribution to free energy g_d, the proposition of [24], which uses the damage variable D and its gradient $\boldsymbol{\nabla} D$, is adopted:

$$g_d(\phi_s, \boldsymbol{\nabla}\phi_s) = \frac{1}{2\rho_0}\frac{G}{L}\ D^2 + \frac{1}{2\rho_0}GL\ \boldsymbol{\nabla} D\cdot\boldsymbol{\nabla} D \tag{44}$$

In the above relation, G and L are material parameters. More specifically, G represents the surface energy density associated with fatigue cracks and L is an internal length controlling the non-local contribution to free energy. In the present work, the non-local contribution to free energy solely depends on the norm of $\boldsymbol{\nabla} D$. The underlying assumption is that the crack surface energy does not depend on the crack orientation. As discussed by Nguyen *et al.* [25] in the context brittle fracture, an anisotropic crack surface energy can be considered by using a tensorial, rather than scalar, parameter for the surface energy density. While the tensorial form is more general, the scalar form is chosen here for simplicity.

The state laws, which connect the different state variables to their dual variables, are obtained by differentiation of the specific Gibbs free energy:

$$s = -\frac{\partial g}{\partial T} = c \ln \frac{T}{T_0} + \frac{1}{T_0} \boldsymbol{\lambda} : \left(\mathbb{S}_0 : \tilde{\boldsymbol{S}} + \boldsymbol{\alpha} \left(T - T_0 \right) \right) \tag{45}$$

$$\boldsymbol{E}_\theta = -\rho_0 \frac{\partial g}{\partial \tilde{\boldsymbol{S}}} = \mathbb{S} : \tilde{\boldsymbol{S}} + \boldsymbol{\alpha} \left(T - T_0 \right) \tag{46}$$

$$X_s = \rho_0 \frac{\partial g}{\partial \alpha_s} = C \alpha_s \tag{47}$$

$$R_s = \rho_0 \frac{\partial g}{\partial \varrho_s} = H \varrho_s^N \tag{48}$$

$$Y_s = \rho_0 \frac{\partial g}{\partial \phi_s} = \frac{G}{L} \, D D_{,\phi_s} - \frac{1}{2} \tilde{\boldsymbol{S}} : \mathbb{S}_{,\phi_s} : \tilde{\boldsymbol{S}} \tag{49}$$

$$\boldsymbol{G}_s = \rho_0 \frac{\partial g}{\partial \boldsymbol{\nabla} \phi_s} = G L D_{,\phi_s} \boldsymbol{\nabla} D \tag{50}$$

According to equation (49), the driving force for the development of damage on the sth slip system Y_s depends on the applied stress tensor $\tilde{\boldsymbol{S}}$ through the derivative of the elastic compliance tensor $\mathbb{S}$ with respect to the corresponding damage variable ϕ_s. According to relation (30), this derivative is:

$$\mathbb{S}_{,\phi_s} = \omega_{,\phi_s} \left(U \left(\sigma_s \right) A_{nn} \mathbb{N}^s_{nn} + A_{nm} \mathbb{N}^s_{nm} + A_{nk} \mathbb{N}^s_{nk} \right) \tag{51}$$

This relation allows reformulating (49) as follows:

$$Y_s = \frac{G}{L} \, D D_{,\phi_s} - \frac{1}{2} \omega_{,\phi_s} \left(U \left(\sigma_s \right) A_{nn} \sigma_s^2 + A_{nm} \tau_s^2 + A_{nk} \pi_s^2 \right) \tag{52}$$

where the shear stresses τ_s and π_s are obtained from the following projections:

$$\tau_s = \boldsymbol{n}_s \cdot \tilde{\boldsymbol{S}} \cdot \boldsymbol{m}_s \tag{53}$$

$$\pi_s = \boldsymbol{n}_s \cdot \tilde{\boldsymbol{S}} \cdot \boldsymbol{k}_s \tag{54}$$

Relation (52) shows that the material parameters A_{nn}, A_{nm} and A_{nk} control the respective contributions of normal and tangential stresses to the development of fatigue damage. Because of closure effects, the contribution of the normal stress σ_s vanishes for negative values.

3.3. Evolution equations

The energy dissipation rate is given by the product of the rate of entropy production and the absolute temperature. The specific dissipation source d is therefore given by:

$$d = \dot{s}T + \frac{1}{\rho_0}\boldsymbol{\nabla}\cdot\boldsymbol{J}T - zT \tag{55}$$

$$= \dot{s}T + \frac{1}{\rho_0}\boldsymbol{\nabla}\cdot\boldsymbol{Q} - \frac{1}{\rho_0}\frac{\boldsymbol{Q}}{T}\cdot\boldsymbol{\nabla}T - r - h \tag{56}$$

Using the local statement of the first law of thermodynamics (9) and the definition (27) of the specific Gibbs free energy, the above relation becomes:

$$\begin{aligned} d = &\frac{1}{\rho_0}\tilde{\boldsymbol{\Sigma}} : \tilde{\boldsymbol{L}}_p - \frac{1}{\rho_0}\sum_s \left(X_s\dot{\alpha}_s + R_s\dot{\varrho}_s + Y_s\dot{\phi}_s + \boldsymbol{G}_s\cdot\boldsymbol{\nabla}\dot{\phi}_s \right) \\ &- \frac{\boldsymbol{Q}}{\rho_0 T}\cdot\boldsymbol{\nabla}T - h \end{aligned} \tag{57}$$

From the expression (50) of the driving force $\boldsymbol{G}_s$ associated with $\boldsymbol{\nabla}\phi_s$, one obtains:

$$\sum_s \boldsymbol{G}_s\cdot\boldsymbol{\nabla}\dot{\phi}_s = GL\sum_s \left(D_{,\phi_s}\boldsymbol{\nabla}D\cdot\boldsymbol{\nabla}\dot{\phi}_s \right) \tag{58}$$

$$= GL\sum_s \left(D_{,\phi_s}\boldsymbol{\nabla}\cdot\left(\boldsymbol{\nabla}D\ \dot{\phi}_s\right) - D_{,\phi_s}\Delta D\ \dot{\phi}_s \right) \tag{59}$$

For the evolution of a material point to be compatible with the second law of thermodynamics, the specific dissipation d must be non-negative (i.e. $d \geq 0$). To comply with this restriction, a convenient choice for the specific power h is:

$$h = -\frac{GL}{\rho_0}\sum_s \left(D_{,\phi_s}\boldsymbol{\nabla}\cdot\left(\boldsymbol{\nabla}D\ \dot{\phi}_s\right)\right) \tag{60}$$

With this choice, the expression of the specific dissipation reduces to:

$$d = \frac{1}{\rho_0}\tilde{\boldsymbol{\Sigma}} : \tilde{\boldsymbol{L}}_p - \frac{1}{\rho_0}\sum_s \left(X_s\dot{\alpha}_s + R_s\dot{\varrho}_s - A_s\dot{\phi}_s \right) - \frac{\boldsymbol{Q}}{\rho_0 T}\cdot\boldsymbol{\nabla}T \tag{61}$$

where the driving force for the development of damage A_s, which includes a non-local contribution, is defined for each slip system according to:

$$A_s = GL\Delta D D_{,\phi_s} - Y_s \tag{62}$$

$$= GL\Delta D D_{,\phi_s} - \frac{G}{L}\ DD_{,\phi_s} + \frac{1}{2}\omega_{,\phi_s}\left(U\left(\sigma_s\right) A_{nn}\sigma_s^2 + A_{nm}\tau_s^2 + A_{nk}\pi_s^2 \right) \tag{63}$$

Within the framework of generalized standard materials, the evolution equations can be obtained from a dissipation potential φ. The dissipation potential φ is a scalar function of the dissipative forces for which the following decomposition of the dissipation

potential is assumed:

$$\varphi\left(\tilde{\boldsymbol{\Sigma}}, X_s, R_s, A_s, \phi_s, \boldsymbol{\nabla} T, T\right) = \varphi_p\left(\tilde{\boldsymbol{\Sigma}}, X_s, R_s\right) + \varphi_d\left(A_s, \phi_s\right) + \varphi_{th}\left(\boldsymbol{\nabla} T, T\right) \tag{64}$$

The plastic contribution φ_p, which solely depends on stress quantities, is:

$$\varphi_p\left(\tilde{\boldsymbol{\Sigma}}, X_s, R_s\right) = \frac{1}{\rho_0} \frac{K}{M+1} \sum_s \left(\frac{\langle |T_s - X_s| - R_s \rangle}{K} \right)^{M+1} \tag{65}$$

where $T_s = \boldsymbol{m}_s \cdot \tilde{\boldsymbol{\Sigma}} \cdot \boldsymbol{n}_s$ is the shear stress acting on the sth slip system and K and M are material parameters. Specifically, K represents the lattice resistance to dislocation motion while the exponent M controls the strain rate-sensitivity.

The contribution φ_d of damage to the dissipation potential is:

$$\varphi_d\left(A_s, \phi_s\right) = \frac{1}{\rho_0} \frac{W}{P+1} \sum_s \left(1 - \phi_s\right) \left(\frac{\langle A_s \rangle}{W} \right)^{P+1} \tag{66}$$

where W and P are material parameters. W is a viscosity-like parameter which controls the resistance to damage development. The rate-dependent character of the damage rule can be adjusted with the parameter P.

Finally, for the thermal part φ_{th} of the dissipation potential, the classical quadratic form is assumed:

$$\varphi_{th}\left(\boldsymbol{\nabla} T, T\right) = \frac{1}{2\rho_0 T} \boldsymbol{\nabla} T \cdot \boldsymbol{\kappa}_0 \cdot \boldsymbol{\nabla} T \tag{67}$$

where $\boldsymbol{\kappa}_0$ is the thermal conductivity tensor in the initial configuration.

The definition of a dissipation potential allows establishing the evolution equations associated with the different internal variables:

$$\tilde{\boldsymbol{L}}_p = \rho_0 \frac{\partial \phi}{\partial \tilde{\boldsymbol{\Sigma}}} = \sum_s \dot{\gamma}_s \boldsymbol{m}_s \otimes \boldsymbol{n}_s \tag{68}$$

$$\dot{\alpha}_s = -\rho_0 \frac{\partial \phi}{\partial X_s} = \dot{\gamma}_s \tag{69}$$

$$\dot{\varrho}_s = -\rho_0 \frac{\partial \phi}{\partial R_s} = |\dot{\gamma}_s| \tag{70}$$

$$\dot{\phi}_s = \rho_0 \frac{\partial \phi}{\partial A_s} = \left(1 - \phi_s\right) \left(\frac{\langle A_s \rangle}{W} \right)^P \tag{71}$$

$$\boldsymbol{Q} = -\rho_0 T \frac{\partial \phi}{\partial \boldsymbol{\nabla} T} = -\boldsymbol{\kappa}_0 \cdot \boldsymbol{\nabla} T \tag{72}$$

where the plastic shear strain rate $\dot{\gamma}_s$ associated with the slip system s is given by:

$$\dot{\gamma}_s = \left(\frac{\langle |T_s - X_s| - R_s \rangle}{K} \right)^M \operatorname{sign}\left(T_s - X_s\right) \tag{73}$$

The proposed constitutive model, which aims at modelling the nucleation and the stage I propagation of fatigue cracks, is formed by the state equations (45) to (50) and

the evolution equations (68) to (72).

4. Spectral method

In the present work, the solution to the field equations resulting from compatibility and static equilibrium (see section 2) is obtained with the spectral method proposed by [26]. The application of this method, which has been extended to the context of finite deformation by [27] and [28], is briefly presented here.

The spectral method is adapted to the situation where the body $\mathcal{B}$ is a volume element submitted to periodic boundary conditions. To benefit from the advantages of Fast Fourier Transform (FFT) techniques, the volume element, whose side dimensions are L_1, L_2 and L_3, is discretized into a regular grid of $N_1 \times N_2 \times N_3$ voxels. An additional assumption consists of considering the temperature field to be both uniform and constant. For this specific case, the history functions $\boldsymbol{\chi}$ and θ have the following forms:

$$\boldsymbol{\chi}(\boldsymbol{X},t) = \bar{\boldsymbol{F}}(t)\cdot\boldsymbol{X} + \tilde{\boldsymbol{\chi}}(\boldsymbol{X},t)\,,\ \theta(\boldsymbol{X},t) = \bar{T} \tag{74}$$

In the above equation, $\bar{\boldsymbol{F}}$ is the prescribed macroscopic deformation gradient tensor, $\tilde{\boldsymbol{\chi}}$ is the periodic contribution to the motion history function and $\bar{T}$ is the imposed temperature. The macroscopic deformation gradient tensor is connected to the deformation gradient field with:

$$\bar{\boldsymbol{F}}(t) = \frac{1}{\mathscr{V}_0}\int_{\mathscr{V}_0} \boldsymbol{F}(\boldsymbol{X},t)\,dV \tag{75}$$

For the application of the spectral method, a homogeneous reference medium, for which the corresponding stiffness tensor is denoted by $\mathbb{L}$, is introduced. The stiffness tensor associated with the homogeneous reference medium allows calculating a polarization field $\delta\boldsymbol{P}(\boldsymbol{X},t)$ from:

$$\delta\boldsymbol{P}(\boldsymbol{X},t) = \boldsymbol{P}(\boldsymbol{X},t) - \mathbb{L}:\boldsymbol{F}(\boldsymbol{X},t) \tag{76}$$

In the absence of volume forces (i.e. $\boldsymbol{B} = \boldsymbol{0}$) and neglecting inertia effects (i.e. $\rho_0\ddot{\boldsymbol{x}} = \boldsymbol{0}$), the local equilibrium condition (6) becomes:

$$(\mathbb{L}:(\boldsymbol{\chi}(\boldsymbol{X},t)\otimes\boldsymbol{\nabla}))\cdot\boldsymbol{\nabla} = -(\delta\boldsymbol{P}(\boldsymbol{X},t))\cdot\boldsymbol{\nabla} \tag{77}$$

The application of the Fourier transform to the above equation leads to[2]:

$$(\mathbb{L}:\boldsymbol{\chi}(\boldsymbol{\xi},t)\otimes\boldsymbol{g}(\boldsymbol{\xi}))\cdot\boldsymbol{d}(\boldsymbol{\xi}) = -\delta\boldsymbol{P}(\boldsymbol{\xi},t)\cdot\boldsymbol{d}(\boldsymbol{\xi}) \tag{78}$$

where $\boldsymbol{\xi}$ is the frequency vector, $\boldsymbol{d}$ (respectively $\boldsymbol{g}$) is the frequency form of the divergence (respectively gradient) operator. In the present work, we adopt the proposition of [29], which consists of using the discrete form of the divergence and gradient oper-

[2]The spatial and frequency forms of a given field Z are differentiated with notations $Z(\boldsymbol{X})$ and $Z(\boldsymbol{\xi})$.

ators, that is:

$$d_j\left(\boldsymbol{\xi}\right) = \frac{N_j}{L_j}\left(1 - \exp\left(-2\pi i \xi_j \frac{L_j}{N_j}\right)\right) \tag{79}$$

$$g_j\left(\boldsymbol{\xi}\right) = \frac{N_j}{L_j}\left(\exp\left(2\pi i \xi_j \frac{L_j}{N_j}\right) - 1\right) \tag{80}$$

The introduction of the acoustic tensor $\boldsymbol{K}$ (with $K_{ik} = \mathbb{L}_{ijkl} g_l d_j$) allows rewriting (77) as follows:

$$\boldsymbol{K}\left(\boldsymbol{\xi}, t\right) \cdot \boldsymbol{\chi}\left(\boldsymbol{\xi}, t\right) = -\delta \boldsymbol{P}\left(\boldsymbol{\xi}, t\right) \cdot \boldsymbol{d}\left(\boldsymbol{\xi}\right) \tag{81}$$

The expression of the deformation gradient tensor in the frequency domain is thus given by:

$$\boldsymbol{F}\left(\boldsymbol{\xi}, t\right) = \begin{cases} \bar{\boldsymbol{F}}\left(t\right), & \boldsymbol{\xi} = \boldsymbol{0} \\ -\mathbb{G}\left(\boldsymbol{\xi}, t\right) : \delta \boldsymbol{P}\left(\boldsymbol{\xi}, t\right), & \boldsymbol{\xi} \neq \boldsymbol{0} \end{cases} \tag{82}$$

where the fourth-rank tensor $\mathbb{G}$ is the modified Green operator (with $\mathbb{G}_{ijkl} = K_{ik}^{-1} g_j d_l$). Relations (76) and (82) are the key for the estimation of the deformation gradient tensor with the spectral method. Indeed, the deformation gradient tensor field is conveniently evaluated in the frequency domain with (82) and then transformed back to the spatial domain. As shown in equation (76), because the polarization field depends on the deformation gradient field, an iterative procedure is required. In this work, the so-called classic scheme proposed by [26] is used.

For a prescribed loading path $\bar{\boldsymbol{F}}\left(t\right)$, the effective response of the volume element is given by the evolution of the macroscopic Piola-Kirchoff stress tensor $\bar{\boldsymbol{P}}\left(t\right)$. According to homogenization theory [30], this stress tensor is simply given by:

$$\bar{\boldsymbol{P}}\left(t\right) = \frac{1}{\mathscr{V}_0} \int_{\mathscr{V}_0} \boldsymbol{P}\left(\boldsymbol{X}, t\right) dV \tag{83}$$

For interface voxels, which correspond to grain boundaries, a specific treatment is adopted. Indeed, the conditions given by equations (3), (5), (8), (10) and (12) should be satisfied for such voxels. The condition (5) is simply enforced by keeping the referential mass density constant. Also, as discussed above, the temperature field is assumed to be spatially homogeneous. As a result of the constitutive equation (72), the heat flux vector and the entropy flux vector are both null. The conditions (10) and (12) are therefore automatically verified. Finally, the composite voxel method of Kabel *et al.* [31] is used to deal with conditions (3) and (8). This method consists in treating an interface voxel as a two phase laminate structure. The two phases have different material properties corresponding to the two sides of the grain boundary. Assuming the stress tensor and the deformation gradient tensor to be piecewice uniform within interface voxels, the stress and deformation gradient tensors of each phase are deduced from equations (3) and (8) as well as constitutive relations. The effective response of the interface voxel is finally obtained from the standard averaging relations of homogenization theory.

Also, as shown in equation (63), the proposed constitutive model requires the determination of ΔD. This field is conveniently evaluated in the frequency domain using

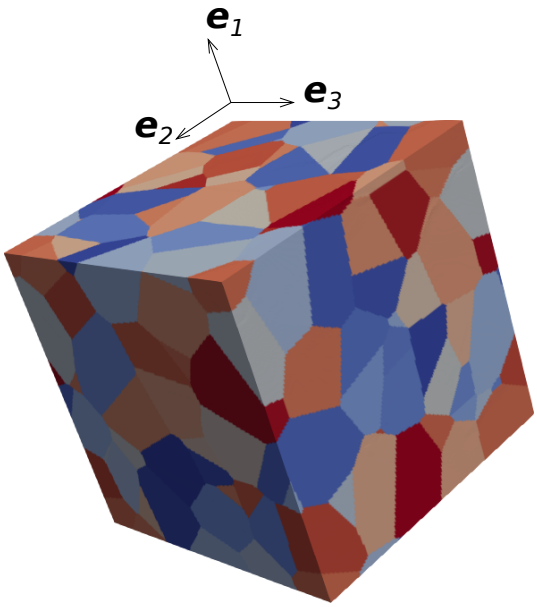

Figure 3. Polycrystalline volume element obtained from a periodic Voronoï tessellation with one hundred grains.

the gradient and divergence operators according to:

$$\Delta D\left(\boldsymbol{\xi},t\right)=D\left(\boldsymbol{\xi},t\right)\boldsymbol{g}\left(\boldsymbol{\xi}\right)\cdot\boldsymbol{d}\left(\boldsymbol{\xi}\right) \tag{84}$$

The inverse Fourier transform is then applied to the above result so that it can be converted to the spatial domain and used for the integration of constitutive relations.

5. Applications

For illustration purposes, the proposed approach is used for investigating the fatigue behavior of a unit volume element (i.e. $L_1 = L_2 = L_3 = 1$ mm). The volume element, which is shown in Figure 3, consists of one hundred equiaxed grains with random crystallographic orientation. Crystallographic slip is restricted to the twelve $\{111\}\langle 110\rangle$ octahedral slip systems. The material parameters used for simulations are listed in Table 2. For the application of the spectral method, the volume element is discretized into $192 \times 192 \times 192$ voxels.

5.1. Cyclic tension test

The case of a strain-controlled uniaxial cyclic tension test is first examined. The corresponding boundary conditions are:

$$\left[\bar{\boldsymbol{F}}\right]=\begin{bmatrix}\bar{F}_{11} & \bullet & \bullet\\ & \bullet & \bullet\\ \text{sym} & & \bullet\end{bmatrix},\ \left[\bar{\boldsymbol{P}}\right]=\begin{bmatrix}\bullet & 0 & 0\\ & 0 & 0\\ \text{sym} & & 0\end{bmatrix}\ \text{and}\ \bar{T}=T_0 \tag{85}$$

Table 2. Material parameters used for the application of the proposed constitutive model. Only independent elastic constants are indicated.

Phenomenon	Parameters			
Elasticity	$\mathbb{C}_{11}$ 159 GPa	$\mathbb{C}_{12}$ 122 GPa	$\mathbb{C}_{44}$ 81 GPa	
Viscoplasticity	K 100 MPa	M 10		
Hardening	H 50 MPa	N 0.1	C 5000 MPa	
Damage	W 0.8 MPa A_{nm} 10^{-5} MPa^{-1}	P 4 A_{nk} 10^{-6} MPa^{-1}	G 1 J/m^2 A_{nn} 10^{-6} MPa^{-1}	L 0.04 mm

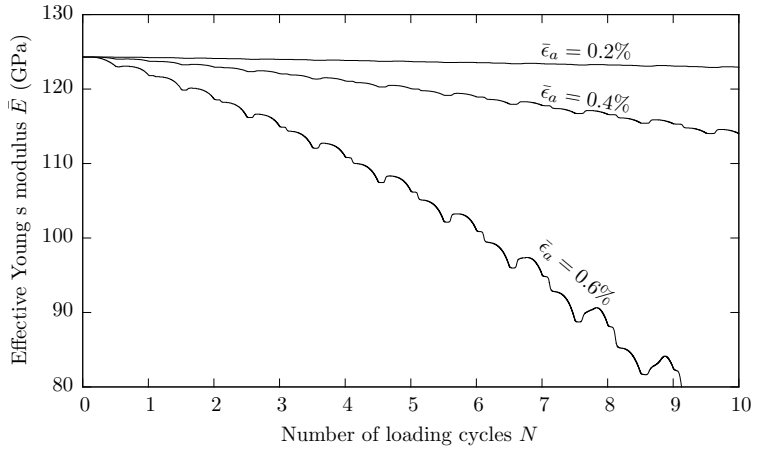

Figure 4. Evolution of the effective Young's modulus $\bar{E}$ along the loading direction as a function of the number of loading cycles N during a cyclic tension test for different strain amplitudes.

where the "$\bullet$" symbol denotes the components of the macroscopic deformation gradient and stress tensors which are free. It should be noticed that both the macroscopic stress tensor $\bar{\boldsymbol{P}}$ and the macroscopic deformation gradient tensor $\bar{\boldsymbol{F}}$ are assumed to be symmetric, so that no macroscopic rigid body rotation is allowed. The axial component of the macroscopic deformation gradient tensor $\bar{F}_{11}$ is such that:

$$\bar{F}_{11} = 1 + \bar{\epsilon}_{11} \tag{86}$$

$$= 1 + \bar{\epsilon}_a \sin(2\pi f t) \tag{87}$$

where $\bar{\epsilon}_a$ is the axial strain amplitude and f is the loading frequency. For the present application, the loading frequency is set to 1 Hz and the strain amplitude is varied from 0.2% to 0.6%.

To evaluate the impact of loading conditions on the accumulation of fatigue damage, the evolution of the effective Young's modulus $\bar{E}$ along the loading direction has been determined for each strain amplitude (see Figure 4). As expected, an increase of the strain amplitude facilitates the development of damage. Also, while the macroscopic Young's modulus $\bar{E}$ globally decreases during cyclic tension tests, some fluctuations are observed during a given loading cycle. Indeed, when the axial stress is reversed toward negative values, the overall stiffness slightly increases because of closure effects.

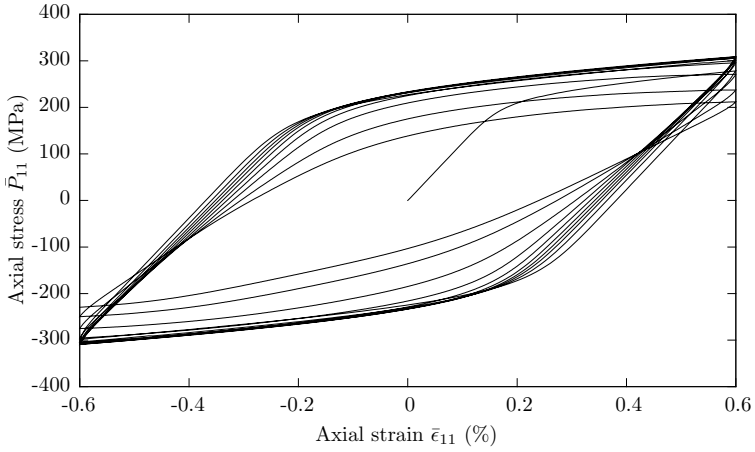

Figure 5. Evolution of the macroscopic axial nominal stress $\bar{P}_{11}$ as a function of the macroscopic axial strain $\bar{\epsilon}_{11}$ during a cyclic tension test for a strain amplitude $\bar{\epsilon}_a$ of 0.6%.

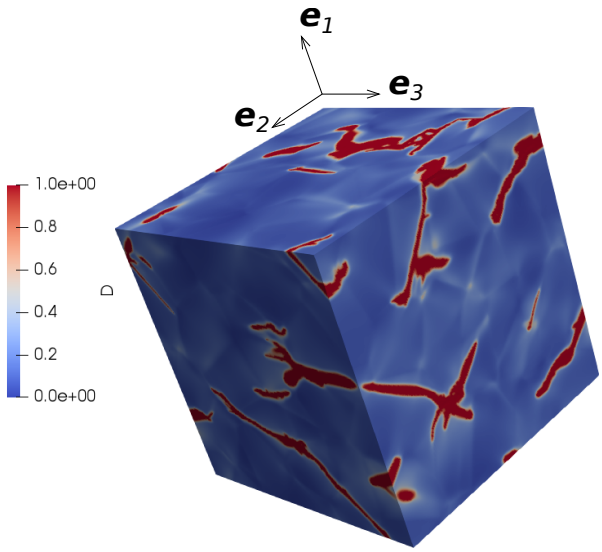

Figure 6. Final damage field D for a cyclic tension test with a strain amplitude $\bar{\epsilon}_a$ of 0.6%.

The axial nominal stress $\bar{P}_{11}$ is plotted as a function of the axial strain $\bar{\epsilon}_{11}$ in Figure 5 for a strain amplitude $\bar{\epsilon}_a$ of 0.6%. Because of the progressive development of damage, an important stress decrease occurs during the last loading cycle. As illustrated by Figure 6, this stress decrease corresponds to the situation where many cracks have nucleated and propagated, which causes an important reduction of the overall stiffness of the volume element.

In polycrystalline materials, grain boundaries are known to be the preferential sites leading to crack initiation [32, 33]. As illustrated by Figure 7, which presents the distribution of the damage variable as a function of the distance to the closest grain boundary d_{GB} for an axial strain amplitude $\bar{\epsilon}_a$ of 0.6%, this aspect is correctly depicted by the proposed model.

Also, according to the experimental work of [34], the candidate zones for crack initiation are those for which a significant amount energy is dissipated into heat. As illustrated by Figure 8, which shows the local amount of heat-dissipated energy per

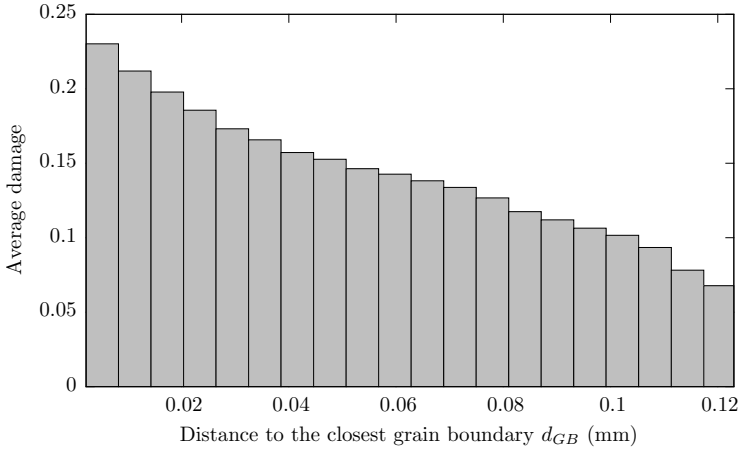

Figure 7. Distribution of the damage variable as a function of the distance to the closest grain boundary d_{GB} for a cyclic tension test with a strain amplitude $\bar{\epsilon}_a$ of 0.6%.

loading cycle[3], the proposed model correctly integrates this aspect.

Finally, to determine on which slip systems fatigue damage is generated, the distribution of the damage variable ϕ_s as a function of the Schmid factor has been plotted in Figure 9. This distribution has been obtained at the end of a cyclic tension test with a strain amplitude $\bar{\epsilon}_a$ of 0.6%. According to the results, the damage variable associated with a given slip system strongly depends on the orientation of the slip system with respect to the loading direction. Specifically, damage preferably develops on slip systems being favourably oriented for slip. This indicates that, though no explicit coupling between plasticity and damage has been considered in the constitutive model, the impact of the crystallographic orientation on the development of fatigue damage is correctly depicted.

5.2. Cyclic shear test

In order to investigate the impact of loading conditions on fatigue damage accumulation, the case of a strain-controlled cyclic shear test is now considered. The boundary conditions used for the simulation of this test are:

$$\left[\bar{\boldsymbol{F}}\right] = \begin{bmatrix} \bullet & \bar{F}_{12} & \bullet \\ & \bullet & \bullet \\ \text{sym} & & \bullet \end{bmatrix}, \ \left[\bar{\boldsymbol{P}}\right] = \begin{bmatrix} 0 & \bullet & 0 \\ & 0 & 0 \\ \text{sym} & & 0 \end{bmatrix} \text{ and } \bar{T} = T_0 \tag{88}$$

with:

$$\bar{F}_{12} = \bar{F}_{21} = \frac{\bar{\gamma}_{12}}{2} \tag{89}$$

$$= \frac{\bar{\gamma}_a}{2} \sin\left(2\pi f t\right) \tag{90}$$

where $\bar{\gamma}_a$ is the shear strain amplitude.

To measure the progression of fatigue damage during cyclic shear tests, the macroscopic shear modulus $\bar{G}$ along the loading direction has been computed for the different

[3]The average dissipated energy density per loading cycle w_d is given by $w_d\left(\boldsymbol{X}\right) = \oint \rho_0\left(\boldsymbol{X}\right) d\left(\boldsymbol{X}, t\right) dt$.

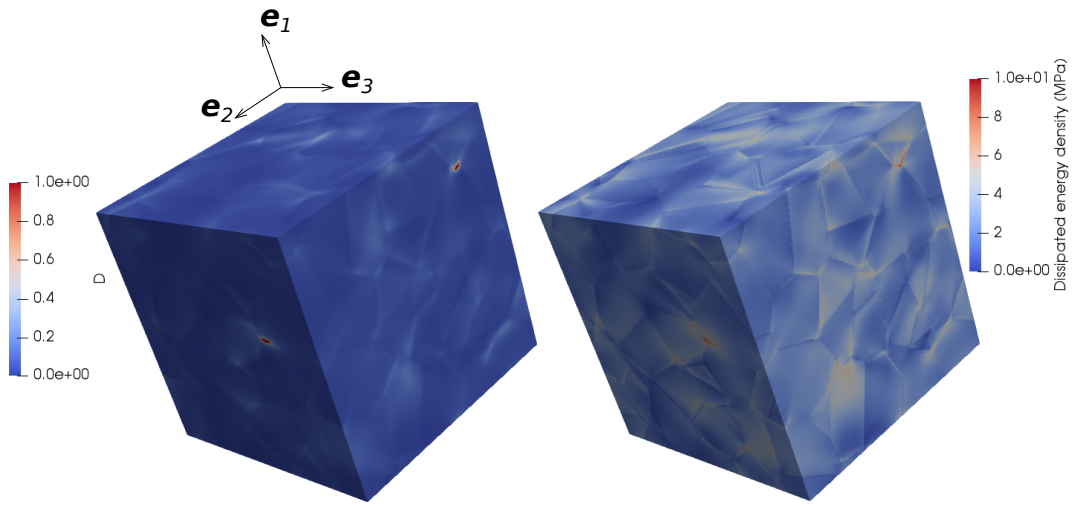

Figure 8. Intermediate damage field D for a cyclic tension test with a strain amplitude $\bar{\epsilon}_a$ of 0.6% (left). Intermediate average dissipated energy density per loading cycle w_d for a cyclic tension test with a strain amplitude $\bar{\epsilon}_a$ of 0.6% (right). The intermediate results have been obtained at the end of the fourth loading cycle (i.e. $N = 4$)

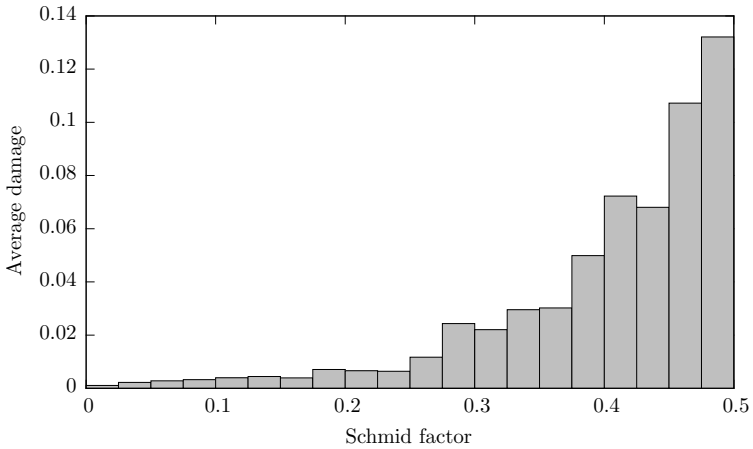

Figure 9. Distribution of the damage variable as a function of the schmid factor for a cyclic tension test with a strain amplitude $\bar{\epsilon}_a$ of 0.6%.

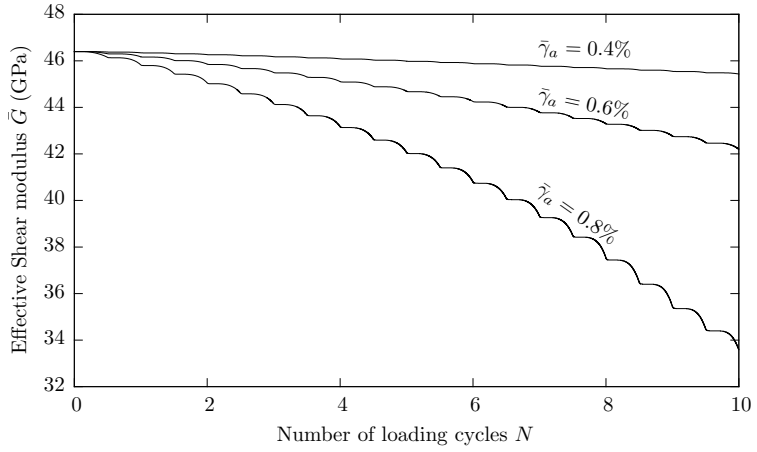

Figure 10. Evolution of the effective shear modulus $\bar{G}$ as a function of the number of loading cycles N during a cyclic shear test for different strain amplitudes.

shear strain amplitudes $\bar{\gamma}_a$ (from 0.4% to 0.8%, see Figure 10). In contrast with cyclic tension tests, the macroscopic shear modulus continuously decreases during a given loading cycle. Indeed, for the specific case of a cyclic shear test, the overall stiffness is less impacted by closure effects since no macroscopic hydrostatic pressure is applied to the volume element.

The final distribution of the damage field, which has been obtained for a shear strain amplitude of 0.8%, is plotted in Figure 11. This distribution is consistent with the experimental observations showing that fatigue cracks preferably develop on planes favorably oriented for crystallographic slip [1].

The present model, which has been formulated in a consistent thermodynamic framework, allows investigating how the energy balance is impacted by fatigue damage. For this purpose, the following average energy densities are defined:

$$\bar{W}_d = \frac{1}{\mathscr{V}_0} \oint \int_{\mathscr{V}_0} \rho_0 d \; dV dt \tag{91}$$

$$\bar{W}_h = \frac{1}{\mathscr{V}_0} \oint \int_{\mathscr{V}_0} \sum_s \left(X_s \dot{\alpha}_s + R_s \dot{\varrho}_s \right) dV dt \tag{92}$$

$$\bar{W}_e = \frac{1}{\mathscr{V}_0} \oint \int_{\mathscr{V}_0} \tilde{\boldsymbol{S}} : \dot{\tilde{\boldsymbol{E}}}_e \; dV dt \tag{93}$$

$$\bar{W}_c = \frac{1}{\mathscr{V}_0} \oint \int_{\mathscr{V}_0} \left(\frac{G}{L} \; D\dot{D} + GL \; \boldsymbol{\nabla} D \cdot \boldsymbol{\nabla} \dot{D} \right) dV dt \tag{94}$$

The average heat dissipated energy density per cycle is denoted by $\bar{W}_d$. The energy densities $\bar{W}_h$, $\bar{W}_e$ and $\bar{W}_c$ provide some information regarding how energy is stored during a loading cycle. Specifically, $\bar{W}_h$ is the contribution of hardening to energy storage, $\bar{W}_e$ is the elastic strain energy accumulated during one loading cycle because of internal stresses and $\bar{W}_c$ is the contribution due to the increase of surface energy associated with the formation of fatigue cracks. These quantites have been computed for a cyclic shear test with a strain amplitude $\bar{\gamma}_a$ of 0.8% (see Figure 12). According to the results, most of the energy provided to the volume element is dissipated into heat, which is consistent with the measurements reported by Bever *et al.* [35] for different

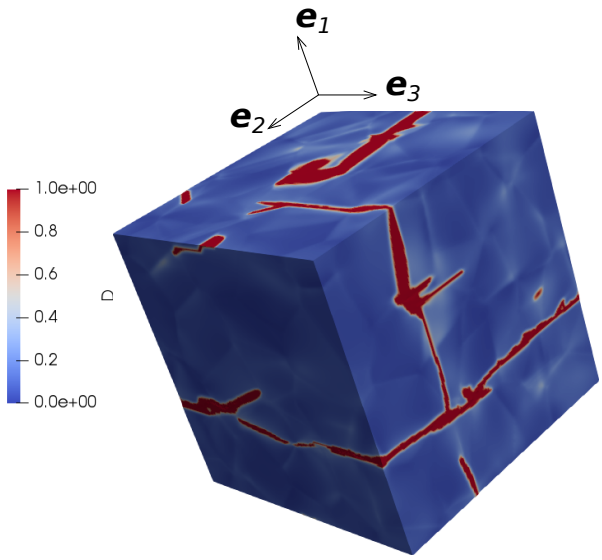

Figure 11. Final damage field D for a cyclic shear test with a shear strain amplitude $\bar{\gamma}_a$ of 0.8%.

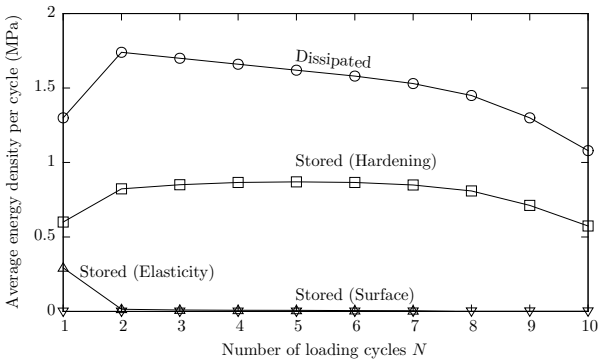

Figure 12. Evolution of the average heat dissipated energy density per cycle and the average stored energy per cycle for a cyclic shear test with a shear strain amplitude $\bar{\gamma}_a$ of 0.8%.

metallic materials. Also, the contribution of damage to energy storage is negligible. Indeed, with the typical values for the surface energy of metals [36], the total crack surface energy is much lower than the energy stored as a result of the microstructural changes (e.g. dislocation multiplication) responsible for hardening.

5.3. Pre-cracked material

The last application focuses on the impact of an initial crack on the fatigue behavior of the polycrystalline volume element. For this purpose, a circular crack of radius 0.15 mm is inserted at the center of the volume element. The loading conditions are the same as in the previous section, thus corresponding to a strain-controlled cyclic shear test (see equation (88)). As shown in Figures 13 and 14, two different cases are examined, depending on the initial crack orientation. In the first case, the crack surface is normal to the $\boldsymbol{e}_1$ direction. For the second case, the crack is perpendicular to the $\boldsymbol{e}_3$ direction. The initial crack is introduced by considering a non-zero initial damage field in the volume element. Specifically, for each voxel with position $\boldsymbol{X}$, the

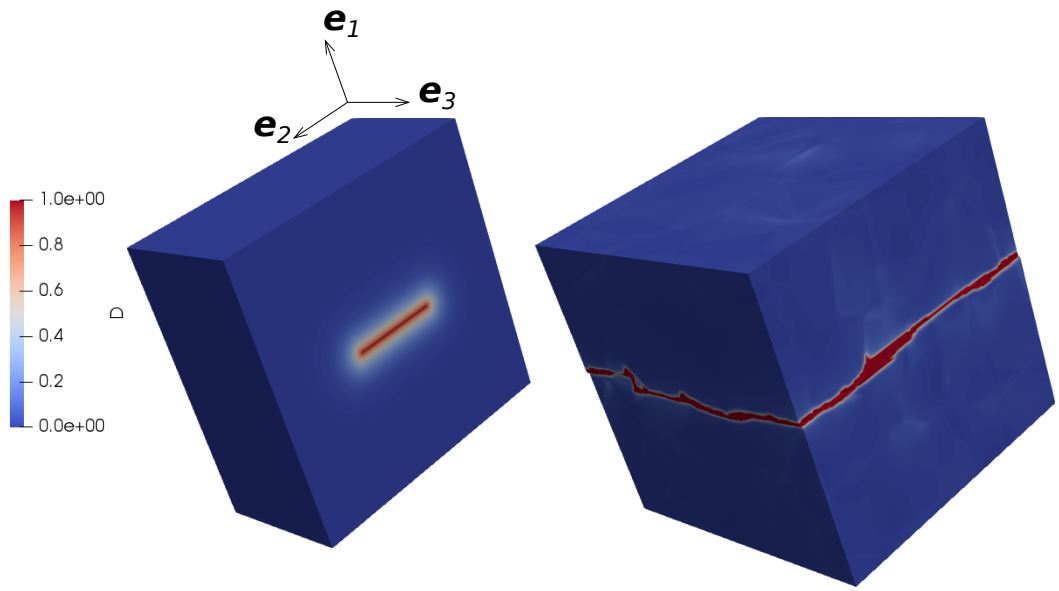

Figure 13. Initial (left) and final (right) damage field D for a cyclic shear test with a shear strain amplitude $\bar{\gamma}_a$ of 0.8%. The initial crack is orthogonal to the $\boldsymbol{e}_1$ direction.

minimum distance to the crack d_c is first calculated with:

$$d_c(\boldsymbol{X}) = \inf\left(\sqrt{(\boldsymbol{X}-\boldsymbol{X}')\cdot(\boldsymbol{X}-\boldsymbol{X}')} \mid \boldsymbol{X}' \in \mathscr{C}_0\right) \tag{95}$$

where $\mathscr{C}_0$ denotes the surface formed by the circular crack in the reference configuration. The initial damage field D is given by:

$$D(\boldsymbol{X},0) = \exp\left(-\frac{d_c(\boldsymbol{X})}{L}\right) \tag{96}$$

If the initial state is assumed to be identical for each system, the damage variable ϕ_s associated with a slip system s is deduced from D with:

$$\phi_s(\boldsymbol{X},0) = \frac{D(\boldsymbol{X},0)}{D(\boldsymbol{X},0) + n\left(1 - D(\boldsymbol{X},0)\right)} \tag{97}$$

This strategy provides an initial damage field that is close to equilibium in the sense that the initial driving force for the growth of damage A_s is negligible.

The evolution of the shear modulus $\bar{G}$ as a function of the number of loading cycles is shown in Figure 15 for a a shear strain amplitude $\bar{\gamma}_a$ of 0.8%. According to the results, damage grows faster in the first case, which corresponds to the situation where the initial crack is contained within the plane with maximum shear stresses. As illustrated by Figure 13, for the first case, the initial crack rapidly extends along the $\boldsymbol{e}_2$ direction, for which shear stresses are maximum. In the second case, damage development is not much impacted by the initial crack. Indeed, for this case, stress concentrations due to microstructural heterogeneities are more critical from the viewpoint of fatigue damage initiation. Fatigue cracks therefore initiate away from the initial crack (see 14).

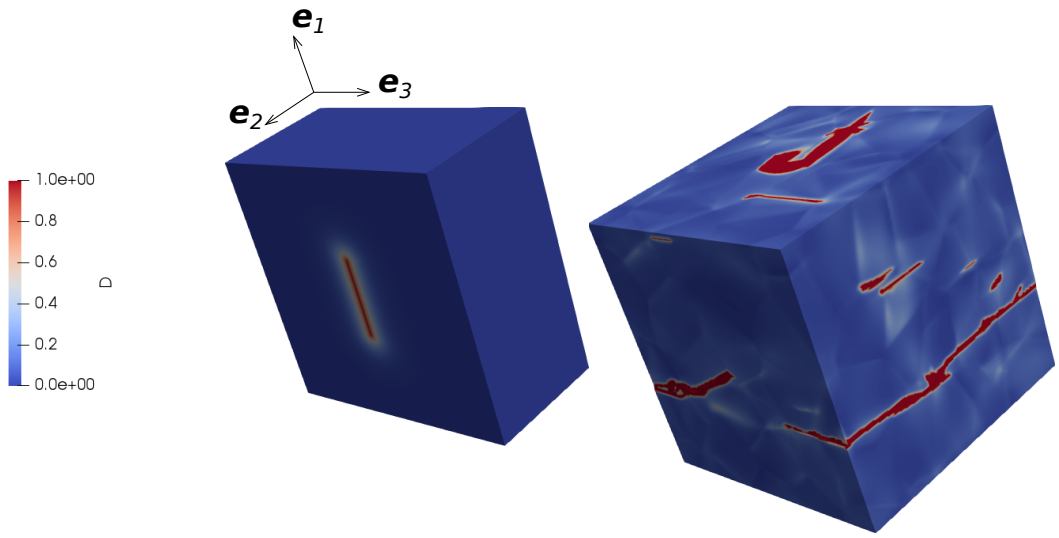

Figure 14. Initial (left) and final (right) damage field D for a cyclic shear test with a shear strain amplitude $\bar{\gamma}_a$ of 0.8%. The initial crack is orthogonal to the $\boldsymbol{e}_3$ direction.

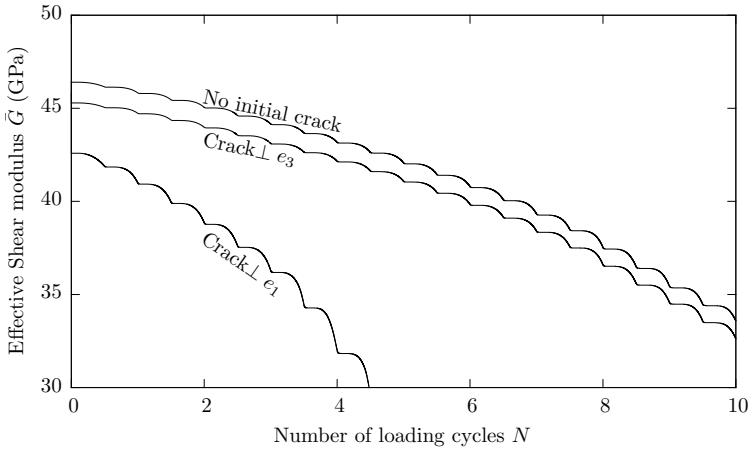

Figure 15. Evolution of the effective shear modulus $\bar{G}$ as a function of the number of loading cycles N during a cyclic shear test for a shear strain amplitude $\bar{\gamma}_a$ of 0.8%.

6. Conclusion

A theoretical framework for modelling fatigue crack nucleation and early growth in polycrystalline materials is proposed. For this purpose, continuum thermodynamics is combined with non-local damage mechanics to construct a set of constitutive relations that explicitly considers the progressive stiffness reduction due to the formation of fatigue cracks. Specifically, a damage variable is attached to each slip system so that the anisotropic aspect of fatigue damage is accounted for. The spatial gradients of the damage variables are treated as additional state variables, which allows considering the increase of surface energy associated with the formation of fatigue cracks. For the evolution equations to be compatible with the second law of thermodynamics, an extra contribution to the entropy flow has been supposed. The constitutive relations have then been implemented in a spectral solver to solve the field equations governing the behavior of a polycrystalline volume element.

For illustration purposes, the proposed model has been used to describe the fatigue behavior of a polycrystalline volume element. According to the numerical results, the impact of the loading mode on the orientation of crack initiation planes is correctly reproduced. Also, because the model is formulated in a consistent thermodynamic framework, the competition between energy dissipation and energy storage during a cyclic deformation process can be investigated. Finally, it allows evaluating the impact of microstructural features (e.g. defects, grain boundaries) on the fatigue behavior of polycrystalline materials.

Future work will focus on the effect of the mean stress state on the fatigue behavior of metallic materials, which is ignored by the proposed model. For this purpose, the possible coupling between hardening variables and damage variables needs to be investigated. As discussed in [15], this coupling is indeed expected to be a key element for the consideration of the influence of the mean stress state.

References

[1] K.S. Chan, *Roles of microstructure in fatigue crack initiation*, Int. J. Fatigue 32 (2010), pp. 1428–1447.

[2] G.M. Castelluccio, D.L. McDowell, *Microstructure-sensitive small fatigue crack growth assessment: Effect of strain ratio, multiaxial strain state, and geometric discontinuities*, Int. J. Fatigue 82 (2016), pp. 521–529.

[3] D.L. McDowell, F.P.E. Dunne, *Microstructure-sensitive computational modeling of fatigue crack formation*, Int. J. Fatigue 32 (2010), pp. 1521–1542.

[4] K. Dang Van. *Sur la résistance à la fatigue des métaux*, Sciences Techniques Armement 3 (1973).

[5] A. Fatemi, D.F. Socie DF, *A critical plane approach to multiaxial fatigue damage including out-of-phase loading*, Fatigue Fract. Eng. Mater. Struct. 11 (1988), pp. 149–65.

[6] C. Przybyla, R. Prasannavenkatesan, N. Salajegheh, D.L. McDowell, *Microstructure-sensitive modeling of high cycle fatigue*, International Journal of Fatigue 32 (2010), pp. 512–525.

[7] Y. Guilhem, S. Basseville, F. Curtit, J.M. Stéphan, G. Cailletaud, *Investigation of the effect of grain clusters on fatigue crack initiation in polycrystals*, International Journal of Fatigue 32 (2010), pp. 1748–1763.

[8] C. Robert, N. Saintier, T. Palin-Luc, F. Morel, *Micro-mechanical modelling of high cycle fatigue behaviour of metals under multiaxial loads*, Mech. Mater. 55 (2012), pp. 112–29.

[9] R. Guerchais, C. Robert, F. Morel, N. Saintier, *Micromechanical study of the loading path*

effect in high cycle fatigue, Int. J. Fatigue 59 (2014), pp. 64–75.
[10] G.M. Castelluccio, D.L. McDowell, *A mesoscale approach for growth of 3D microstructurally small fatigue cracks in polycrystals*, Int J Damage Mech 23 (2014), pp. 791–818.
[11] G.M. Castelluccio, D.L. McDowell, *Mesoscale modeling of microstructurally small fatigue cracks in metallic polycrystals*, Materials Science & Engineering A 598 (2014), pp. 34–55.
[12] J. Lemaitre, *A Course on Damage Mechanics*, Springer-Verlag, Berlin, 1996.
[13] V. Monchiet, E. Charkaluk, D. Kondo, *Plasticity-damage based micromechanical modelling in high cycle fatigue*, C. R. Mecanique 334 (2006), pp. 129–136.
[14] J. Zghal, H. Gmati , C. Mareau, F. Morel, *A crystal plasticity based approach for the modelling of high cycle fatigue damage in metallic materials*, International Journal of Damage Mechanics 25 (2016), pp. 611–628.
[15] C. Mareau, F. Morel, *A continuum damage mechanics-based approach for the high cycle fatigue behavior of metallic polycrystals*, International Journal of Damage Mechanics (2018), pp. 1–19.
[16] G.A. Maugin, W. Muschik, *Thermodynamics with Internal Variables. Part I. General Concepts*, J. Non-Equilib. Thermodyn. 19 (1994), pp 217–249.
[17] R. de Borst, J. Pamin , M.G.D. Geers, *On coupled gradient-dependent plasticity and damage theories with a view to localization analysis*, Eur. J. Mech. A/Solids 18 (1999), pp. 939–962.
[18] M. Frémond, B. Nedjar, *Damage, gradient of damage and principle of virtual power*, Int. J. Solids and Structures 33 (1996), pp. 1083–1103.
[19] G.A. Maugin, *Internal Variables and Dissipative Structures*, J. Non-Equilib. Thermodyn. 15 (1990), pp 173–192.
[20] P. Germain, Q.S. Nguyen, P. Suquet, *Continuum thermodynamics*, Journal of Applied Mechanics 50 (1983), pp. 1010–1020.
[21] P. Ireman, Q.S. Nguyen, *Using the gradients of temperature and internal in Continuum Thermodynamics*, C. R. Mecanique 332 (2004), pp. 249–255.
[22] E. H. Lee, *Elastic-plastic deformation at finite strains*, J. Appl. Mech. 36 (1969), pp. 1–6.
[23] Q. Chen, H.W. Liu, Resolved shear stress intensity coefficient and fatigue crack growth in large crystals, Theoretical and Applied Fracture Mechanics 10 (1988), pp. 111–122.
[24] C. Miehe, F. Welschinger, M. Hofacker, *Thermodynamically consistent phase-field models of fracture: Variational principles and multi-field FE implementations*, Int. J. Numer. Meth. Engng 83 (2010), pp. 1273–1311.
[25] T.T. Nguyen, J. Réthoré, J. Yvonnet, M.C. Baietto, *Multi-phase-field modeling of anisotropic crack propagation for polycrystalline materials*, Computational Mechanics 60 (2017), pp. 289–314.
[26] H. Moulinec, P. Suquet, *A numerical method for computing the overall response of nonlinear composites with complex microstructure*, Comput. Methods Appl. Mech. Engrg. 157 (1998), pp. 69–94.
[27] N. Lahellec, J .C. Michel, H. Moulinec, P. Suquet, *Analysis of inhomogeneous materials at large strains using Fast Fourier Transforms*, in *Computational Mechanics of Solid Materials at large Strains*, C. Miehe, ed., Kluwer Academic Press, Stuttgart, 2003, pp. 247–258.
[28] P. Eisenlohr, M. Diehl, R.A. Lebensohn, F. Roters, *A spectral method solution to crystal elasto-viscoplasticity at finite strains*, International Journal of Plasticity 46 (2013), pp. 37–53.
[29] F. Willot, *Fourier-based schemes for computing the mechanical response of composites with accurate local fields*, C. R. Mecanique 343 (2015), pp. 232–245.
[30] R. Hill, *On constitutive macro-variables for heterogeneous solids at finite strain*, Proc. R. Soc. Lond. A. 326 (1972), pp. 131–147.
[31] M. Kabel, A. Fink, M. Schneider, *The composite voxel technique for inelastic problems*, Computer Methods in Applied Mechanics and Engineering 322 (2017), pp. 396–418.
[32] R. Chang, *A dislocation mechanism of grain boundary crack nucleation and growth under low cyclic stresses*, Scripta Metall. 13 (1979), pp. 1079–1081.

[33] H.J. Christ, *On the orientation of cyclic-slip-induced intergranular fatigue cracks in face-centered cubic metals*, Mater. Sci. Engng A 117 (1989), pp. L25–L29.
[34] B. Berthel, B. Wattrisse, A. Chrysochoos, A. Galtier, *Thermographic Analysis of Fatigue Dissipation Properties of Steel Sheets*, Strain 43 (2007), pp. 273–279.
[35] M.B. Bever, D.L., Holt, A.L.,Titchener, A. L., *The stored energy of cold work*, Progress in Materials Science 7 (1973), pp. 5–177.
[36] L. Vitos, A.V. Ruban, H.L. Skriver, J. Kollár, *The surface energy of metals*, Surface Science 411 (1998), pp. 186–202.